Enhancement of peri-implant bone osteogenic activity induced by a peptidomimetic functionalization of titanium

View Letter

Close

Date: Jan 24, 2018
To: "Francesca Ravanetti" francesca.ravanetti@unipr.it
cc: degirola@unina.it;sonja.hammer@web.de
From: "Annals of Anatomy" eesserver@eesmail.elsevier.com
Reply To: "Annals of Anatomy" friedrich.paulsen@fau.de
Subject: Your Submission

Ms. Ref. No.: AANAT2709R1
Title: Enhancement of peri-implant bone osteogenic activity induced by a peptidomimetic functionalization of titanium
Annals of Anatomy

Dear Dr. Ravanetti,

I am pleased to inform you that your paper "Enhancement of peri-implant bone osteogenic activity induced by a peptidomimetic functionalization of titanium" has been accepted for publication in Annals of Anatomy.

Thank you for submitting your work to Annals of Anatomy.

Yours sincerely,

Friedrich Paulsen
Editor-in-Chief
Annals of Anatomy

****

For further assistance, please visit our customer support site at http://help.elsevier.com/app/answers/list/p/7923. Here you can search for solutions on a range of topics, find answers to frequently asked questions and learn more about EES via interactive tutorials. You will also find our 24/7 support contact details should you need any further assistance from one of our customer support representatives.

Close

Annals of ANATOMY

Contact us
Help ?

home | main menu | submit paper | guide for authors | register | change details | log out

Username: francesca.ravanetti@unipr.it
Switch To: Author Go to: My EES Hub

Version: EES 2018.3

Submissions with an Editorial Office Decision for Author Francesca Ravanetti

Page: 1 of 1 (2 total completed submissions)

Display 10 results per page.

Action	Manuscript Number	Title	Initial Date Submitted	Status Date	Current Status	Date Final Disposition Set	Final Disposition
Action Links	AANAT2073	EFFECT OF THE SUPPLEMENTATION OF A BLEND CONTAINING SHORT AND MEDIUM CHAIN FATTY ACID MONOGLYCERIDES IN MILK REPLACER ON RUMEN PAPILLAE DEVELOPMENT IN WEANING CALVES.	Oct 29, 2015	May 13, 2016	Completed - Accept	May 13, 2016	Accept
Action Links	AANAT2709	Enhancement of peri-implant bone osteogenic activity induced by a peptidomimetic functionalization of titanium	Oct 31, 2017	Jan 24, 2018	Accept		

Page: 1 of 1 (2 total completed submissions)

Display 10 results per page.

Enhancement of peri-implant bone osteogenic activity induced by a peptidomimetic functionalization of titanium

Ravanetti F[1]., Gazza F[1]., D'Arrigo D[1]., Graiani G[2]., Zamuner A[3]., Zedda M[4]., Manfredi E[2]., Dettin M[3]. and Cacchioli A[1].

[1] Dept. of Veterinary Sciences, [2] Dept. of Medicine and Surgery, University of Parma, [3] Dept. of Industrial Engineering, University of Padova, [4] Dept. of Veterinary Medicine, University of Sassari.

(*) Corresponding author:

Dr. Francesca Ravanetti

Department of Veterinary Sciences,

University of Parma, Via del Taglio, 10, 43126, Parma, Italy

Keywords:

Peptidomimetic functionalization, histomorphometry, bone deposition, bone markers, rat.

Abstract

Osteoblast cell adhesion to the extracellular matrix is established through two main pathways: one is mediated by the binding between integrin and a minimal adhesion sequence (RGD) on the extracellular protein, the other is based on the interactions between transmembrane proteoglycans and heparin-binding sequences found in many matrix proteins.

The aim of this study is the evaluation in an in vivo endosseous implant model of the early osteogenic response of the peri-implant bone to a biomimetic titanium surface functionalized with the retro-inverso 2DHVP peptide, an analogue of Vitronectin heparin binding site. The experimental plan is based on a bilateral study design of Control and 2DHVP implants inserted respectively in the right and left femur distal metaphysis of adult male Wistar rats (n=16) weighing about 300 gr and evaluated after 15 days.

Fluorochromic bone vital markers, were given at specific time frame, in order to monitor the dynamic of new bone deposition. The effect inducted by the peptidomimetic coating on the surrounding bone were qualitatively and quantitatively evaluated by means of static and dynamic histomorphometric analyses performed within three concentric and subsequent circular Regions of Interest (ROI) of equivalent thickness (220 μm), ROI1 adjacent to the interface, ROI2, the middle, and ROI3 the farthest. The data indicated that these functionalized implants stimulated a higher bone apposition rate ($p<0,01$) and larger and rapid osteoblast activation in terms of mineralising surface within ROI1 compared to the Control ($p<0,01$). These higher osteoblast recruitment and activation leads to a greater bone to implant contact reached for DHVP samples ($p<0,5$). This represents an initial stimulus of the osteogenic activity that might results in a faster and better osteointegration process.

1. Introduction

Osteoblasts are anchorage-dependent cells: several functions, such as proliferation, migration, differentiation, bone matrix deposition and mineralization, strictly depend on the adhesion process. This process is mediated and activated by the extracellular proteins; in case of foreign materials, cells do not adhere directly to it, but via the protein adsorbed on the material surface (Brunette, D.M.; Tengvall, P.; Textor, Marcus; Thomsen, 2001). For this reason, extracellular matrix (ECM) composition may be useful in tailoring biomaterials to stimulate tissue-specific cellular responses. In fact, each ECM protein may regulate several different behaviors of the cells including adhesion, migration, proliferation and differentiation by interacting with specific cell receptors. Re-creating the biological signals derived from the ECM by attaching bone ECM-specific protein domain onto the titanium surface, could be a powerful strategy to design new peptidomimetic surfaces (Shekaran and García, 2011). Bone cells adhere to a wide variety of extracellular matrix proteins and this process is a key point in bone development, repair, and disease (Brighton and Albelda, 1992). Considered the important regulatory role that ECM molecules play on cellular responses in vivo, several full-length ECM proteins have been studied for coating bone implants in the bone defect healing approach. Attempts were made with collagen (Morra et al., 2005; Rammelt et al., 2006; Schliephake et al., 2005; Svehla et al., 2005), fibrin (Ben-Ari et al., 2009; Karp et al., 2004; Kim et al., 2007), hyaluronic acid (Barros et al., 2009; Paderni et al., 2009; Solchaga et al., 1999), decellularized matrix (Kurkalli et al., 2010; Suckow et al., 1999) as well as bone sialoprotein (Graf et al., 2008). The existing limitations in using full-length ECM molecules have spurred the use of peptide mimicry approach; peptides or recombinant fragments derived from their parent ECM protein by incorporating the minimal functional sequence able to maintain the bioactivity of the original protein. In fact, all of the extracellular molecules disclose in their primary structure one or more consensus sequences, long few peptides, that can be recognized by specific cell receptor. When these receptors recognize and bind the numerous ECM components they are able to discern, they cluster together on the cell membrane and form a macromolecular structure, called focal adhesion.

In particular, the majority of the interaction between bone cells and extracellular matrix proteins is mediated by integrins, a widely expressed family of transmembrane receptors, formed by a non-covalent association of an α and a β subunit (Robey, PG; John, PB; Lawrence, GR; Gideon, 2002). Osteoblasts and osteoprogenitors cells express different types of integrins, like α1β1, α2β1, α3β1, α4β1, α5β1, α6β1, α8β1 or αvβ34. The L-arginine, glycine, and L-aspartic acid (Arg-Gly-Asp or RGD) is the minimal adhesion sequence recognized by integrin receptors and it has been found in many ECM proteins. For the biomimetic functionalization of biomaterials, several peptides

containing the RGD sequence have been developed and studied. However, the integrin-mediated adhesion process was demonstrated to be not selective for osteoblasts, but widely used by other cell types.

Another important adhesion process in bone cells is established through interactions between transmembrane proteoglycans, like heparan sulfate proteoglycan (HSPG), and heparin-binding sequences found in many ECM proteins (Dalton et al., 1995). These types of interactions might also be considerable to control the behaviour of osteoprogenitor cells (Dee et al., 1998). A great number of evidence support the significant involvement of HSPGs in osteoblast adhesion. For example, heparan sulfate was detected immunohistochemically on the membrane of osteoblasts attached to the bone matrix (Nakamura and Ozawa, 1994). Furthermore, blocking the heparin-binding sites of fibronectin with Platelet Factor IV, inhibited approximately 45% of the subsequent osteoblast adhesion (Puleo and Bizios, 1992). Moreover, heparan sulfate added in the culture medium completely inhibited human bone-derived cell attachment to the heparin-binding region of fibronectin (Dalton et al., 1995) and the adhesion of osteoblasts to osteoactivin coated matrix was significantly inhibited by heparin, whereas the same concentration of heparin had no effect on cell attachment to fibronectin (Moussa et al., 2014). Studies focusing on the identification of bioactive peptides able to promote the osteoblast adhesion via the heparan sulfate pattern are much more recent and less studied. Dettin et al. found and developed the peptide reproducing the 351-359 sequence of human vitronectin, called HVP (Dettin et al., 2002; Vacatello et al., 2005) and demonstrated its specificity for bone cells and its ability in promoting *in-vitro* the osteoblast adhesion on surfaces functionalized with it (Dettin et al., 2005). Subsequent studies focused on the optimisation of the functionalisation method for creating biomimetic implantable devices. Two different methods were tested, the first was a silica gel as resorbable peptide carrier (Dettin et al., 2006), the second was the peptide covalent bond on titanium substrates (Bagno et al., 2007b). The covalent coating method resulted the best performing one, considering the physical-chemical properties and the cell in vitro behaviour, morphology and the gene expression analysis (Brun et al., 2013). The (351-359)HVP covalently functionalized titanium cylinders were in-vivo studied in rabbits to evaluate the effect of functionalisation on the osteogenic activity. The results demonstrated that the peptide enhanced the osteogenic activity accelerating the bone neodeposition in a short time frame after implantation (Cacchioli et al., 2009). Numerous experimental reads out supporting the biological activity of the (351-359) peptide were achieved, however in solution the peptide sequence resulted degraded by the trypsin (Zamuner et al., 2017). For this reason, the biomimetic peptide was fine-tuned; the new approach was based on the design of a dimeric form, in order to increase the peptide ionic interactions with cellular GAGs, and its retro-inverted analogue

consisting in the reversed amino acids sequence composed of D-amino acids (Zamuner et al., 2017). In-vitro studies demonstrated that the dimeric form of this peptide, called 2DHVP, maintained an optimal adhesive ability and matrix mineralization induction (Giovine, M, Dettin, M, Castagliuolo, 2016). The aim of this study is the evaluation, in an in vivo endosseous implant model, of the early osteogenic response of the peri-implant bone to the biomimetic titanium surface functionalized with the dimeric form of the adhesive, retro-inverso 2DHVP peptide.

2. Materials and Methods

2.1 Materials

Sieber Amide resin and all Fmoc- protected amino acids were from Novabiochem (Merck KGaA, Darmstadt, Darmstadt, Germany). The coupling reagents 2-(1H-Benzotriazole-1-yl)-1,1,3,3-tetramethyluronium hexafluorophosphate (HBTU) and 1-Hydroxybenzotriazole (HOBt) were from Advanced Biotech (Seveso, MI, Italy). N,N-diisopropylethylamine (DIPEA) and piperidine were from Biosolve (Leenderweg, Valkenswaard, The Netherlands). Triethoxysilane (TES) was from Sigma-Aldrich (Steinheim, Germany). Solvents such as N,N-dimethylformamide (DMF), trifluoroacetic acid (TFA), N-methyl-2- pyrrolidone (NMP), dichloromethane (DCM), and acetonitrile were from Biosolve.

2.2 Synthesis of side chain-protected 2DHVP

The synthetic peptide 2DHVP (sequence: H–D-Tyr–Gly–D-Lys–D-Arg–D-Asn–D-Arg–D-His–D-Arg–D-Phe–D-Tyr–Gly–D-Lys–D-Arg–D-Asn–D-Arg–D-His–D-Arg–D-Phe –NH2) is the retro-inverted form of HVP dimer (sequence of HVP dimer: H-Phe-Arg-His-Arg-Asn-Arg-Lys-Gly-Tyr-Phe-Arg-His-Arg-Asn-Arg-Lys-Gly-Tyr-NH2).

The peptide 2DHVP was produced by solid-phase peptide synthesis approach (synthesizer Syro I, MultisynTech, Witten, Germany), using Fmoc chemistry. Super acid labile Sieber Amide resin (1748 mg, 0.125 mmol, substitution 0.72 mmol/g) was loaded in the reactor. The following side chain protections were used: Trt, His and Asn; Boc, Lys; But, Tyr; Pmc, Arg. After the synthesis, the peptide was cleaved from the solid support without the deprotection of side chains by 5 treatments with a 1% TFA/DCM solution for 5 min. The side-chain protected peptide (sequence:H–D-Tyr(But)–Gly–D-Lys(Boc)–D-Arg(Pmc)–D-Asn(Trt)–D-Arg(Pmc)–D-His(Trt)–D-Arg(Pmc)–D-Phe–D-Tyr(But)–Gly–D-Lys(Boc)–D-Arg(Pmc)–D-Asn(Trt)–D-Arg(Pmc)–D-His(Trt)–D-Arg(Pmc)–D-Phe–NH2) was precipitated with cold water.

2.3 Titanium implants preparation

Commercially pure titanium (Ti grade 2) implants (diameter, 2 mm; height, 2.3 mm;) were obtained from cylindrical bars by turning. First, they were smoothed with grit paper, then sand-blasted (corundum 450 mm for 10 s), and finally attacked with acidic solution: hydrogen chloride (HCl) (36%v/v)/sulphuric acid (98%v/v)/water (H2O) (1/1/3) for 6 min at mixture boiling point (Bagno et al., 2007a). Afterwards, sand-blasted and acid-attacked (SLA) cylinders were thoroughly degreased, washed, and sonicated in a sequence of solvents: water, acetone and toluene.

2.4 Titanium implants functionalization

Oxidized samples were treated at 25° C for 2 h with a solution consisting of equal volumes of concentrated H_2SO_4 and 30 % aqueous H_2O_2 under magnetic stirring. The cylinders were then cleaned with water and acetone and dried under vacuum.

Silanization of oxidized samples was performed by heating them for 4 h in refluxing toluene containing 10 % (3-aminopropyl)triethoxysilane (Nanci et al., 1998). Silanized samples were used as controls. After washing with toluene and drying under vacuum, the implants were immersed in a solution of 10 mg glutaric anhydride and 5 ml DIPEA in 40 mL of NMP over 4 h. The implants were washed with NMP (3 times, 1 min each) and acetone (3 times, 1 min each), then dried under vacuum for 1 h.

The side-chain-protected peptide was anchored by immersion of the implants in a solution prepared with 40 mg side chains –protected peptide, 5 mg HBTU, 2 mg HOBt, 7.5 µL DIPEA in 15 mL NMP for 21 h (Dettin et al., 2009). The implants were washed with NMP (3 times, 1 min each) and ethanol (3 times, 1 min each), then dried under vacuum for 15 min.

The side chain deprotection of the peptides anchored to the implant surface was carried out by treatment with 0.25 mL EDT, 0.1 mL TES, 0.23 mL H2O in 10 mL TFA for 1 h. The following washes were performed: TFA (1 time, 1 min); acetone (2 times, 1 min each); MilliQ water (3 times, 1 min each); acetone (2 times, 1 min each) (Figure 1). Finally, the implants were dried under vacuum for 15 min. Sterilization of 2DHVP and control samples were carried out with 70% alcoholic solution treatment for 5 min, followed by 20 min under UV lamp.

2.5 Surgical procedure

The experimental plan consisted of 16 adult male outbred rats (Rattus Norvegicus, Wistar strain - Charles River Laboratories, Wilmongton, MA), weighing about 300 gr. European and Italian regulations on animal experimentation were strictly followed during the entire study, according to the European Commission rules (European Union 86/609 CEE–Health Ministry Authorisation N. 274/2016 of 16/03/2016).

Rats were stabulated at a 22-24°C, with light-dark cycle of 12/12 h, feeding with pellets food and water *ad libitum* were acclimated for 7 days, prior to start the experiment.

Surgical procedure was performed under general anaesthesia; the antibiotic coverage was performed with sub-cutaneous administration of Enrofloxacin (Baytryl, 10-20 mg/kg) and the analgesia was carried out with Carprofen (Rymadil, 5 mg/Kg). Once the animal was anaesthetized (Zoletil 100, Virbac, 30 mg/Kg), the skin and subcutaneous tissues were incised exposing the lateral portion of the femur's distal metaphysis. In each femur the implantation site was created proximally to the lateral non articular elevation on condyles lateralis by means of a trephine burr of 2.0 mm

external diameter, under abundant irrigation with sterile saline. The implants were press-fitted into the implant site following the bilateral study design; the peptide-grafted implant (2DHVP) in the left femur, while oxidized and silanized implant (CTRL) in the right one, as internal control. Soft tissues were then repositioned and then animals were sutured (Vycril Ethicon 5.0, Johnson&Johnson, Amersfoort, Netherlands) (Figure 2 A-F).

To evaluate the osteogenic activity, two vital bone markers (Pautke et al., 2005; Rahn and Perren, 1971) were administered intraperitoneally at sequential time frame: Calcein Green (CG, 5 mg/kg; Sigma, St. Louis, MO) at the 7th and 8th day after the surgery, and Xylenol Orange (XO, 90 mg/kg; Sigma) at the 12th and 13th day (Figure 2G). At the end of the experimental period, at the 15th day after surgery, animals were sacrificed by an anaesthetic overdose (Pentothal Sodium, 5 mg/kg).

2.6 Histology

Immediately after the sacrifice, the distal portion of each femur containing the implant was harvested and fixed in 10% neutral buffered formalin solution (Histo-Line Laboratories, Pantigliate, Italy) for 48 hours. Specimens were then dehydrated in three ascending alcoholic solutions (70%, 95%, 100%) (Histo-Line Laboratories) and infiltrated in methyl methacrylate resin, Osteo-Bed (Polysciences, Warrington, PA). To activate the radicalic polymerization the benzoyl peroxide was added as catalyst and samples maintained at 34°C for 48/72 hours. Serial sections, 60-90 µm thick, perpendicular to the major axis of the implants were obtained with rotative microtome (Leica 1600, Leica Biosystems, Nussloch, DE) equipped with a diamond blade. Skeletal landmarks have been maintained during the bone sectioning.

To evaluate the morphology of periimplant bone, corresponding sections for each sample, was stained with Goldner's trichrome and Villanueva staining (Polysciences). Sections were analysed with bright field and polarized light microscopy for histological and static histomorphometry and with fluorescence microscopy for dynamic histomorphometry. Analysis were performed by means of a motorized microscope (Nikon Eclipse 90i), equipped with a digital camera (Nikon model 5 M) connected to an image analysis software (NIS—Elements AR 3.10; Nikon, Japan). The acquisition of the images was carried out under previously standardized exposition, gain and magnifications.

2.7 Static and dynamic histomorphometry

To quantitatively evaluate the newly formed bone at the bone-to-implant interface and to compare the data between CTRL and 2DHVP functionalized implants both static and dynamic histomorphometric analysis were performed.

By means of the binary tool of the image analysis software, we created three concentric and subsequent circular Regions Of Interest (ROI) of equivalent thickness (220 µm), realized starting from the end of the implant profile. ROI1 was the closest region to the device surface, ROI2, was the middle, and ROI3 was the farthest (Figure 6A).

The following parameters have been considered (Giavaresi et al., 2003; Overgaard et al., 2000; Parfitt, 1988; Recker, 1983; Schnitzler and Mesquita, 2006):

- Bone-to-implant contact (%) [BIC]: measured in bright field as the ratio between the length of the bone segments in direct contact with the surface of the implant and the length of the implant perimeter. It was also measured in fluorescent microscopy [Osteogenic BIC], as the ratio between the length of the active osteogenic front in direct contact with the implant surface for both Calcein Green and Xylenol Orange and the length of the implant perimeter.
- Mineral apposition rate for single label (µm/day) [MAR-SL]: evaluated for both Calcein Green and Xylenol Orange, it was calculated within the ROI1 as the ratio between the average thickness of the marked osteogenic fronts and the period of the administration of the respective bone vital marker.
- Mineralizing surface versus bone surface (%) [MS/BS]: evaluated for both vital bone markers as the ratio between the surface marked with the relative marker, assessed in fluorescence microscopy, and the total bone surface in the region of interest, assessed in bright field microscopy.

An Intensity Surface Plot transformation based on the computational evaluation, by the microscope software, of the single pixel intensity values were applied to the fluorescence images. The BIC and MAR-SL parameters were manually measured within only the first ROI, while the MS/BS was semi-automatically calculated in all the three ROIs as means of a customized computerized macro, specifically designed for the ROIs. The ROIs were further divided in quadrants according to the reference direction Distal-Caudal, Distal-Cranial, Proximal-Caudal and Proximal-Cranial (Figure 6C) to evaluate whether the bone neodeposition had a preferential direction.

2.8 Statistical analysis

The number of experimental animals was calculated by A-Priori Power Analysis (G*Power Version 3.1.2; Franz Faul, University of Kiel, DE) and authorised by the Minister with the Ministry Authorisation N. 274/2016 of 16/03/2016.

Static and dynamic histomorphometric data were analysed by means of one-way analysis of variance (ANOVA) and Tukey's multiple comparison test, with the statistical tool SPSS v.24.0 (SPSS, Chicago, IL) prior angular transformation of the values (because all the data were expressed as quotients and not as natural numbers).

Data are reported as means ± standard error and plotted as histograms, with significance $p<0.05$.

3. Results

3.1 Post surgery recovery and Gross Anatomy

All the animals showed a good recovery after the surgery: the weight, the response to nutrition and hydration, as well as the deambulation resumed quickly to the physiological levels. From the gross morphology inspection only one rat displayed a muscular hematoma, but not affecting the bone periosteum. In all the animals, the implants appeared correctly located in the lateral portion of the femur's distal metaphysis, the periosteum was intact and the surrounding tissue appeared unaffected.

The linear distance from the articular face of the lateral condyle to the implant resulted uniform indicating that the devices were all well positioned in the anatomical site.

3.2 Histology

The analysis with bright field microscopy allow to assess the histological features of the periimplant bone in term of quality of the bone and the extracellular matrix, bone to implant interface maintenance, presence of inflammatory infiltrates and connective fibrotic tissue around the implant.

In both functionalized (2DHVP) and control (CTRL) groups at the end of the experimental time, bone neo-formation was observed: as shown in Figure 3 thin spicules originated from the pre-existing bone surfaces headed toward the implant-bone interface, forming a thin layer of new bone that allowed the implant primary stabilisation. From a morphologic point of view, the newly formed bone had the typical morphology of a primary woven bone tissue, with large and roundish lacunae and osteocytes and weaved collagen fibers organization (Figure 3 A,B,E,F). The presence of inflammatory infiltrate and the deposition of fibrous tissue at the interface was excluded for both 2DHVP and CTRL groups. The polarized light microscopy showed bright and dark areas indicating the irregular collagen fibers organization and mineralisation of the matrix (Figure 3 C,G). From a qualitative point of view, the osteogenic induction seemed to be greater in the functionalized group compared to the control group. Villanueva Bone Staining, assessing the quality and the cellularity of the new deposed bone, also confirmed the histological outcomes. The tissue in close proximity to the implant resulted to be a low-density bone, stained in red, or a moderately permeable bone, stained in orange-brown, meaning that it was recently synthetized and not yet remodeled. Several osteoid seams front, stained in green and located on the edge of the newly synthetized bone, were detected in the proximity of bone-implant interface (Figure 3 D,H).

The analysis in fluorescence microscopy allowed to investigate the osteogenic effect induced by the surface treatments at the interface during the administration period. The Calcein Green (CG) labelling, administered on the 7th and 8th day after surgery, appeared linear and continuous on several osteogenic fronts in both the groups. The Xylenol Orange (XO) labelling, administered on the 12th and 13th day from the surgery, exhibited a lower spread signal with a pattern less elongated on the fronts and more punctiform. Figure 4 shows a representative merged fluorescence images of the two bone markers for CTRLs and 2DHVPs; from a qualitative approach the Calcein Green signal from the 2DHVP group seemed to be more intense in the closest region to the implant compared to that from CTRLs, meanwhile the signals originated from Xylenol Orange seemed to be equal among the surfaces. These observations become even more evident applying to those images an Intensity Surface Plot transformation, based on the plotting of each single pixel intensity values (Figure 4C,D).

3.3 Static and Dynamic histomorphometry

The histomoprhometric results were grouped, summarised in Table 1 and graphed in figures as average value ± the standard error.

3.3.1 Bone to Implant Contact (BIC)

The histomorphometric static parameter Bone to Implant Contact (BIC) quantified the bone amount and deposition at the bone-implant interface and represents an index of the osteointegrative ability of a biomaterial.

We measured this parameter at the end of the experimental time and in the two fluorescent bone markers time frame. Comparing the obtained results from the two different surfaces, higher values emerged from the 2DHVP groups compared to those from the CTRLs group.

At the end of the experimental time, 15 days after surgery, the BIC of 2DHVP surface exhibited a significantly higher ($p = 0.11$) bone-implant contact compared to the CTRL group (Figure 5A).

In addition, the osteogenic BIC, evaluated in fluorescence microscopy, calculated for the functionalized surfaces showed higher values in the Calcein Green time frame compared to the CTRL ones, and this difference was statistically significant ($p=0,002$). On the contrary, in the Xylenol Orange time frame, no statistical difference was found between 2DHVP and CTRL groups ($p=0,566$) (Figure 5 B).

3.3.2 Mineral Apposition Rate for Single Label (MAR-SL)

This dynamic histomorphometric parameter measured in the periimplant bone revealed for CG marker a statistically lower rate of deposition ($p = 0,002$) in the CTRL group as compared to the

2DHVP group; for the XO marker, again statistically higher values (p = 0,016) were revealed for the 2DHVP samples compared to those of the CTRL samples (p=0,016), even if their difference resulted smaller (Figure 5 C).

Comparing the trend of the MAR in the two markers time frame, it was possible to note that the MAR-CG values were the highest in both the groups. Overall, the mineral apposition rate reached its maximum at the 8th day after the surgery and then decreased tending to be aligned with the CTRL value in the second experimental time. Even if the treated value remained significantly higher, it experimented a greater decrease compared to that experimented by the controls (Figure 5C).

3.3.3 Mineralizing surface versus bone surface (%) [MS/BS]:

The parameter Mineralizing surface versus bone surface measured within the ROI1 indicated significantly higher values (p = 0,012) reached by 2DHVP as compared to CTRL for the CG marker, but this difference was not revealed for the XO marker. The readout at the CG time frame were higher compared to those of the XO time frame, and the maximum value was reached, consistent with the other parameters, by the treated group (Figure 6B).

The data obtained within the ROI2, showed a different trend: no statistically significant difference at the Calcein Green (CG) time frame between 2DHVP and CTRLs was observed. Furthermore, the MS/BS values of both CTRL and 2DHVP groups decreased tending to align themselves, although the treated samples experimented the greater decrease, while maintaining higher value. The data from the XO remained clearly smaller and almost equal between the two surfaces. The trend of the ROI3 (Figure 6B) remained substantially the same of that from ROI2. No statistical difference resulted between the 2DHVP and CTRL groups and all the values decreased for both the markers. The data from this region tended mainly to match themselves toward minimal values. The comparison of the values obtained from both the markers within the three ROIs exhibited an activation gradient starting from the implant surface only in the treated group for the Calcein Green marker. As it is shown in Figure 6, the percentage of the active mineralizing bone in those samples was maximum in the first ROI and then decreased regularly in direct relation to the increase of the distance from the implant surface. The statistical analysis confirmed this gradient demonstrating that it was a peculiar feature of the 2DHVP group. In fact, the 2DHVP values for the CG marker resulted significantly different in the three ROIs; the first ROI was significantly different compared to that from the second (p=0,032) and from the third (p=0,003) ROI. Instead, the difference between ROI2 and ROI3 for 2DHVP samples at the CG time frame did not have statistical relevance

(p=0,653). On the contrary, for the CTRL groups considering the same marker time frame, the values among the three ROIs was not supported by any significant difference.

The analysis of MS/BS subdivided according to the reference direction Distal-Caudal, Distal-Cranial, Proximal-Caudal and Proximal-Cranial showed a higher bone deposition for the treated group and no one preferential neodeposition direction of the periimplant bone (Figure 6D).

4. Discussion

In the recent years the research of the biomaterials field was primarily focused on the micro and nanostructure control of surfaces and on the biofunctionalization with bioactive molecules capable of establish a tight communication with the cells, influencing their phenotype, adhesion or growth.

In the last decade a new biologically active peptide reproducing the 351-359 sequence of human vitronectin, called HVP, was developed (Dettin et al., 2002; Vacatello et al., 2005) and demonstrated to be able and specific only for bone cells to promote *in-vitro* the osteoblast adhesion on functionalized surfaces (Dettin et al., 2005). Successive studies focused on the research of the most efficient functionalisation method for creating biomimetic implantable devices; the peptide covalent bond on titanium substrates (Bagno et al., 2007a) resulted the best performing one, considering the physico-chemical properties, the cell morphologic studies and the gene expression analysis (Brun et al., 2013). Once the covalently functionalized method had been chosen, the (351-359)HVP covalently functionalized titanium cylinders were created for an *in-vivo* study in rabbits (Cacchioli et al., 2009). Results demonstrated that the implant surface functionalized with HVP peptide enhanced *in vivo* the osteogenic activity immediately after the implantation, accelerating the bone growth at the interface.

As a drawback, the peptide sequence resulted *in-vitro* partially degraded in the presence of serum, in particular by the trypsin (Giovine, M, Dettin, M, Castagliuolo, 2016). For this reason, the same biomimetic peptide, with a chemistry implemented for degradation resistance was developed. The new approach was based on the use of D-amino acids in the synthesis of a retro-inverso peptide reproducing the same sequence of the (351-359)HVP. *In-vitro* studies demonstrated that the dimeric form of this peptide, called 2DHVP, maintained the same adhesive ability and the same degree of matrix mineralization and significantly improved the expression of three bone marker proteins(Giovine, M, Dettin, M, Castagliuolo, 2016). The present work aimed to evaluate in an *in-vivo* bone model the osteogenic properties of the peptidomimetic approach based on the titanium functionalization with the 2DHVP retro-inverso peptide.

A short experimental time of 15 days was selected for the study based on previous data indicating that the implants coated with HVP peptide reached the maximum osteogenic activity shortly after

the surgery (Cacchioli et al., 2009; Dettin et al., 2005) in particular after 9 days in a rabbit model. The histologic outcome revealed newly deposed primary woven bone characterised by weave collagen fibres organization and big and numerous osteocytes with a round shape and irregular arborisation of their canalicular network at the bone to implant interface.

The fluorescent microscopy confirms the osteogenic activity at the interface and on the bone spicule edges. The quantitative histomoprhometric analysis has revealed higher values in the 2DHVP samples compared to the CTRL ones for all the parameters.

The BIC parameter is significantly improved in the 2DHVP group compared to that of the CTRLs, meaning that there is more bone tissue in direct contact with the 2DHVP implant surface then in the CTRLs one, confirming the *in vivo* effect of the biomimetic peptide (Cacchioli et al., 2009; Novaes et al., 2010) . The BIC readout resulted in accordance with previous studies, presenting slightly higher values, due to the different animal model used, rat instead of rabbit, and due to implantation site used, femur condyles lateralis instead of distal femur epiphysis.

Considering the osteogenic BIC, for Calcein Green time frame the 2DHVP surfaces shows significantly higher values compared to the CTRL ones, whilst on the contrary, for Xylenol Orange time frame, no statistical difference was found between the two surfaces. Probably, this difference emerges because the induction effect of the peptide revealed at the CG time frame was going down with the advancement of experimental time. Overall, the results for this parameter demonstrated a greater new bone amount and deposition at the bone-implant interface, meaning a higher early osteointegrative ability for the 2DHVP functionalized implants.

Also the MAR-SL analysis confirmed an higher deposition rate reached at the CG time frame by the 2DHVP group, resulting significantly greater compared to those of the CTRLs group. Moving from the CG to the XO time frame, a clear decrease of MAR is noticeable, even if the 2DHVP values remain significantly higher than the others. These results comply with previous results (Cacchioli et al., 2009), in which it was demonstrated that the MAR-SL reached their peak 9 days after the surgery in the functionalized implant, decreasing at the 16th day. The parameter mineralizing surface versus bone surface for Calcein Green bone marker showed a statistically significant difference between 2DHVP and CTRLs only within ROI1. Within the other two ROIs, further from the surface, no significant difference between the two groups is observed, demonstrating the localized action of the peptide on osteogenic activity. The bioactivity of the (351-359)HVP sequence, on which the 2DHVP sequence is based, has already been associated with an increased osteogenic activity in the closest region to the implant immediately after the surgery (Cacchioli et al., 2009; Lüthen et al., 2005).

Additional evidence of the pro-osteogenic role of the peptidomimetic functionalisation is that no significant difference is found in any ROIs of the CTRLs samples excluding any significant osteogenic effect induced by the implant surgery itself. The implant insertion provoked a damage in the tissue, with the consequent activation of the physiologically healing process in both the groups; in the 2DHVP group the decreasing trend of MS/BS moving from ROI1 to ROI3 resulted greater, as compared to that observed for CTRLs group, due to the effect on osteogenic activity induced by peptide.

The same parameter analysed for Xylenol Orange resulted significantly lower as compared to those calculated for Calcein Green, at CG time frame and no difference emerged among ROIs demonstrating that the peptide had a short-time frame activation effect.

Even if a direct comparison with previous study is not possible due to experimental differences, the here reported results confirms the previous findings, strengthened by the detection of significant difference between the two surfaces.

As a consequence of the European and national restriction of the regulations on animal experimentation and in order to increase the sample size for statistical reasons we changed the animal model from rabbit to rat. Regarding the anatomical site, a previous work (Omar et al., 2011) demonstrated that once that the steady-state is reached after the surgery, the expression of bone formation markers (Alkaline Phosphatase and Osteocalcin) and bone resorption markers (tartrate-resistant acid phosphatase and cathepsin K) is significantly higher in the femur distal portion compared with the proximal and distal tibia. On the contrary, the expression of pro-inflammatory markers (Tumor Necrosis Factor alpha and Interleukin 1 beta) resulted significantly lower in the femur compared to both proximal and distal tibia. As anatomical location the distal epiphysis was used as in the previous studies, but the implant site was adapted to the rat as selected animal model based on the fact that rat femurs are smaller, and the lateral portion of the distal metaphysis resulted more suitable for biomechanical and bone microarchitecture reasons.

5. Conclusions

The peptidomimetic surface functionalisation of titanium implant or endosseous biomaterials represents a recent strategy to control and modulate the bone to implant-interface. The optimisation of the (351–359)HVP peptide to avoid partial peptide degradation by serum trypsin has been reached developing the dimeric retro-inverso form of this peptide sequence, named 2DHVP. The present study demonstrated the *in vivo* orthotopic pro-osteogenic effect of 2DHVP functionalization of titanium implant. reported The histological and histomorphometrical outcomes indicated that the

functionalized implants have a significantly higher bone apposition rate (MAR-SL) and a significantly larger and rapid osteoblast activation in terms of MS/BS within ROI1 compared to the CTRLs, that reaches its peak 8 days after the surgery.

These elements together led to a higher osteogenic BIC values for 2DHVP samples than for CTRLs already from the CG time frame (8 days after surgery) and then confirmed at the end of experimental time (15 days). The titanium implants functionalized with the 2DHVP peptide, stimulating the osteoblast adhesion at the interface, enhanced the osteogenic activity immediately after implantation and accelerated the deposition of newly formed periimplant bone.

Considering the promising results here reported, in the near future it will investigated both the peptide activity in ectopic site and the orthotopic osteogenic activity on more advanced preclinical models. Due to its mechanism of action, the application of this peptidic biomimetic functionalization is extremely interesting as coating for endosseous implants while it finds little applicability in case of bone defects.

References

Bagno, A., Piovan, A., Dettin, M., Brun, P., Gambaretto, R., Palù, G., Di Bello, C., Castagliuolo, I., 2007a. Improvement of Anselme's adhesion model for evaluating human osteoblast response to peptide-grafted titanium surfaces. Bone 41, 704–712. https://doi.org/10.1016/j.bone.2007.06.008

Bagno, A., Piovan, A., Dettin, M., Chiarion, A., Brun, P., Gambaretto, R., Fontana, G., Di Bello, C., Palù, G., Castagliuolo, I., 2007b. Human osteoblast-like cell adhesion on titanium substrates covalently functionalized with synthetic peptides. Bone 40, 693–699. https://doi.org/10.1016/j.bone.2006.10.007

Barros, R.R.M., Novaes, A.B., Papalexiou, V., Souza, S.L.S., Taba, M., Palioto, D.B., Grisi, M.F.M., 2009. Effect of biofunctionalized implant surface on osseointegration - A histomorphometric study in dogs. Braz. Dent. J. 20, 91–98. https://doi.org/10.1590/S0103-64402009000200001

Ben-Ari, A., Rivkin, R., Frishman, M., Gaberman, E., Levdansky, L., Gorodetsky, R., 2009. Isolation and implantation of bone marrow-derived mesenchymal stem cells with fibrin micro beads to repair a critical-size bone defect in mice. Tissue Eng. Part A 15, 2537–46. https://doi.org/10.1089/ten.tea.2008.0567

Brighton, C.T., Albelda, S.M., 1992. Identification of integrin cell-substratum adhesion receptors on cultured rat bone cells. J. Orthop. Res. 10, 766–73. https://doi.org/10.1002/jor.1100100604

Brun, P., Scorzeto, M., Vassanelli, S., Castagliuolo, I., Pal??, G., Ghezzo, F., Messina, G.M.L., Iucci, G., Battaglia, V., Sivolella, S., Bagno, A., Polzonetti, G., Marletta, G., Dettin, M., 2013. Mechanisms underlying the attachment and spreading of human osteoblasts: From transient interactions to focal adhesions on vitronectin-grafted bioactive surfaces. Acta Biomater. 9, 6105–6115. https://doi.org/10.1016/j.actbio.2012.12.018

Brunette, D.M.; Tengvall, P.; Textor, Marcus; Thomsen, P., 2001. Titanium in Medicine. Springer-Verlag Berlin Heidelb. 1019.

Cacchioli, A., Ravanetti, F., Bagno, A., Dettin, M., Gabbi, C., 2009. Human Vitronectin-Derived Peptide Covalently Grafted onto Titanium Surface Improves Osteogenic Activity: A Pilot In Vivo Study on Rabbits. Tissue Eng. Part A 15, 2917–26. https://doi.org/10.1089/ten.TEA.2008.0542

Dalton, B. a, McFarland, C.D., Underwood, P. a, Steele, J.G., 1995. Role of the heparin binding domain of fibronectin in attachment and spreading of human bone-derived cells. J. Cell Sci. 108 (Pt 5, 2083–2092.

Dee, K.C., Andersen, T.T., Bizios, R., 1998. Design and function of novel osteoblast-adhesive peptides for chemical modification of biomaterials. J. Biomed. Mater. Res. 40, 371–377. https://doi.org/10.1002/(SICI)1097-4636(19980605)40:3<371::AID-JBM5>3.0.CO;2-C

Dettin, M., Bagno, A., Morpurgo, M., Cacchioli, A., Conconi, M.T., Di Bello, C., Gabbi, C., Gambaretto, R., Parnigotto, P.P., Pizzinato, S., Ravanetti, F., Guglielmi, M., 2006. Evaluation of silicon dioxide-based coating enriched with bioactive peptides mapped on human vitronectin and fibronectin: In vitro and in vivo assays. Tissue Eng. 12. https://doi.org/10.1089/ten.2006.12.3509

Dettin, M., Conconi, M.T., Gambaretto, R., Bagno, A., Di Bello, C., Menti, A.M., Grandi, C.,

Parnigotto, P.P., 2005. Effect of synthetic peptides on osteoblast adhesion. Biomaterials 26, 4507–4515. https://doi.org/10.1016/j.biomaterials.2004.11.023

Dettin, M., Conconi, M.T., Gambaretto, R., Pasquato, A., Folin, M., Di Bello, C., Parnigotto, P.P., 2002. Novel osteoblast-adhesive peptides for dental/orthopedic biomaterials. J. Biomed. Mater. Res. 60, 466–471. https://doi.org/10.1002/jbm.10066

Dettin, M., Herath, T., Gambaretto, R., Iucci, G., Battocchio, C., Bagno, A., Ghezzo, F., Di Bello, C., Polzonetti, G., Di Silvio, L., 2009. Assessment of novel chemical strategies for covalent attachment of adhesive peptides to rough titanium surfaces: XPS analysis and biological evaluation. J. Biomed. Mater. Res. - Part A 91, 463–479. https://doi.org/10.1002/jbm.a.32222

Giavaresi, G., Fini, M., Cigada, a, Chiesa, R., Rondelli, G., Rimondini, L., Aldini, N.N., Martini, L., Giardino, R., 2003. Histomorphometric and microhardness assessments of sheep cortical bone surrounding titanium implants with different surface treatments. J. Biomed. Mater. Res. A 67, 112–120. https://doi.org/10.1002/jbm.a.10044

Giovine, M, Dettin, M, Castagliuolo, I., 2016. Smart Biomaterials: attività biologica di sequenze peptidiche retro-inverse resistenti alla degradazione proteolitica per la funzionalizzazione covalente specifcia di superfici implantari. Universtà degli Studi di Padova.

Graf, H.-L., Stoeva, S., Armbruster, F.P., Neuhaus, J., Hilbig, H., 2008. Effect of bone sialoprotein and collagen coating on cell attachment to TICER and pure titanium implant surfaces. Int. J. Oral Maxillofac. Surg. 37, 634–40. https://doi.org/10.1016/j.ijom.2008.01.021

Karp, J.M., Sarraf, F., Shoichet, M.S., Davies, J.E., 2004. Fibrin-filled scaffolds for bone-tissue engineering: An in vivo study. J. Biomed. Mater. Res. - Part A 71, 162–171. https://doi.org/10.1002/jbm.a.30147

Kim, S.J., Jang, J.D., Lee, S.K., 2007. Treatment of long tubular bone defect of rabbit using autologous cultured osteoblasts mixed with fibrin. Cytotechnology 54, 115–120. https://doi.org/10.1007/s10616-007-9084-1

Kurkalli, B.G.S., Gurevitch, O., Sosnik, A., Cohn, D., Slavin, S., 2010. Repair of bone defect using bone marrow cells and demineralized bone matrix supplemented with polymeric materials. Curr. Stem Cell Res. Ther. 5, 49–56.

Lüthen, F., Lange, R., Becker, P., Rychly, J., Beck, U., Nebe, J.G.B., 2005. The influence of surface roughness of titanium on beta1- and beta3-integrin adhesion and the organization of fibronectin in human osteoblastic cells. Biomaterials 26, 2423–40. https://doi.org/10.1016/j.biomaterials.2004.07.054

Morra, M., Cassinelli, C., Meda, L., Fini, M., Giavaresi, G., Giardino, R., 2005. Surface analysis and effects on interfacial bone microhardness of collagen-coated titanium implants: a rabbit model. Int. J. Oral Maxillofac. Implants 20, 23–30.

Moussa, F.M., Hisijara, I.A., Sondag, G.R., Scott, E.M., Frara, N., Abdelmagid, S.M., Safadi, F.F., 2014. Osteoactivin promotes osteoblast adhesion through HSPG and alphavbeta1 integrin. J. Cell. Biochem. 115, 1243–1253. https://doi.org/10.1002/jcb.24760

Nakamura, H., Ozawa, H., 1994. Immunohistochemical localization of heparan sulfate proteoglycan in rat tibiae. J. Bone Miner. Res. 9, 1289–1299. https://doi.org/10.1002/jbmr.5650090819

Nanci, A., Wuest, J.D., Peru, L., Brunet, P., Sharma, V., Zalzal, S., McKee, M.D., 1998. Chemical

modification of titanium surfaces for covalent attachment of biological molecules. J. Biomed. Mater. Res. 40, 324–335. https://doi.org/10.1002/(SICI)1097-4636(199805)40:2<324::AID-JBM18>3.0.CO;2-L

Novaes, A.B., de Souza, S.L.S., de Barros, R.R.M., Pereira, K.K.Y., Iezzi, G., Piattelli, A., 2010. Influence of implant surfaces on osseointegration. Braz. Dent. J. https://doi.org/10.1590/S0103-64402010000600001

Omar, O., Suska, F., Lennerås, M., Zoric, N., Svensson, S., Hall, J., Emanuelsson, L., Nannmark, U., Thomsen, P., 2011. The Influence of Bone Type on the Gene Expression in Normal Bone and at the Bone-Implant Interface: Experiments in Animal Model. Clin. Implant Dent. Relat. Res. 13, 146–156. https://doi.org/10.1111/j.1708-8208.2009.00195.x

Overgaard, S., Søballe, K., Jørgen, H., Gundersen, G., 2000. Efficiency of systematic sampling in histomorphometric bone research illustrated by hydroxyapatite-coated implants: optimizing the stereological vertical-section design. J. Orthop. Res. 18, 313–321. https://doi.org/10.1002/jor.1100180221 [doi]

Paderni, S., Terzi, S., Amendola, L., 2009. Major bone defect treatment with an osteoconductive bone substitute. Musculoskelet. Surg. 93, 89–96. https://doi.org/10.1007/s12306-009-0028-0

Parfitt, A.M., 1988. Bone histomorphometry: standardization of nomenclature, symbols and units. Summary of proposed system. Bone Miner. 4, 1–5.

Pautke, C., Vogt, S., Tischer, T., Wexel, G., Deppe, H., Milz, S., Schieker, M., Kolk, A., 2005. Polychrome labeling of bone with seven different fluorochromes: Enhancing fluorochrome discrimination by spectral image analysis. Bone 37, 441–445. https://doi.org/10.1016/j.bone.2005.05.008

Puleo, D.A., Bizios, R., 1992. Mechanisms of fibronectin-mediated attachment of osteoblasts to substrates in vitro. Bone Miner. 18, 215–226. https://doi.org/10.1016/0169-6009(92)90808-Q

Rahn, B.A., Perren, S.M., 1971. Xylenol Orange, a fluorochrome useful in polychrome sequential labeling of calcifying tissues. Biotech. Histochem. 46, 125–129. https://doi.org/10.3109/10520297109067836

Rammelt, S., Illert, T., Bierbaum, S., Scharnweber, D., Zwipp, H., Schneiders, W., 2006. Coating of titanium implants with collagen, RGD peptide and chondroitin sulfate. Biomaterials 27, 5561–5571. https://doi.org/10.1016/j.biomaterials.2006.06.034

Recker, R.R., 1983. Bone Histomorphometry: Techniques and Interpretations. CRC Press.

Robey, PG; John, PB; Lawrence, GR; Gideon, A., 2002. Bone Matrix Proteoglycans and Glycoproteins., in: Princ. Bone Biol. Vol 2. San Diego Acad. Press, pp. 225–237.

Schliephake, H., Aref, A., Scharnweber, D., Bierbaum, S., Roessler, S., Sewing, A., 2005. Effect of immobilized bone morphogenic protein 2 coating of titanium implants on peri-implant bone formation. Clin. Oral Implants Res. 16, 563–569. https://doi.org/10.1111/j.1600-0501.2005.01143.x

Schnitzler, C.M., Mesquita, J.M., 2006. Cortical bone histomorphometry of the iliac crest in normal black and white South African adults. Calcif. Tissue Int. 79, 373–382. https://doi.org/10.1007/s00223-006-0053-z

Shekaran, A., García, A.J., 2011. Extracellular matrix-mimetic adhesive biomaterials for bone

repair. J. Biomed. Mater. Res. - Part A. https://doi.org/10.1002/jbm.a.32979

Solchaga, L.A., Dennis, J.E., Goldberg, V.M., Caplan, A.I., 1999. Hyaluronic acid-based polymers as cell carriers for tissue-engineered repair of bone and cartilage. J. Orthop. Res. 17, 205–213. https://doi.org/10.1002/jor.1100170209

Suckow, M.A., Voytik-Harbin, S.L., Terril, L.A., Badylak, S.F., 1999. Enhanced bone regeneration using porcine small intestinal submucosa. J. Investig. Surg. 12, 277–287. https://doi.org/10.1080/089419399272395

Svehla, M., Morberg, P., Bruce, W., Walsh, W.R., 2005. No effect of a type I collagen gel coating in uncemented implant fixation. J. Biomed. Mater. Res. - Part B Appl. Biomater. 74, 423–428. https://doi.org/10.1002/jbm.b.30256

Vacatello, M., D'Auria, G., Falcigno, L., Dettin, M., Gambaretto, R., Di Bello, C., Paolillo, L., 2005. Conformational analysis of heparin binding peptides. Biomaterials 26, 3207–3214. https://doi.org/10.1016/j.biomaterials.2004.09.009

Zamuner, A., Brun, P., Scorzeto, M., Sica, G., Castagliuolo, I., Dettin, M., 2017. Smart biomaterials: Surfaces functionalized with proteolytically stable osteoblast-adhesive peptides. Bioact. Mater. 2, 121–130. https://doi.org/10.1016/j.bioactmat.2017.05.004

Table 1. Results of the histomorphometric analysis for 2DHVP and CTRLs groups. The dynamic parameters were analysed in their proper time frame, corresponding to that of marker administration: 7-8 days (Calcein Green), 12-13 days (Xylenol Orange). The static parameters were analysed at 15 days that is the end of the experimental time. The measured parameters were: Bone to Implant Contact (BIC), measured both in bright field and in fluorescence microscopy; Mineral Apposition Rate for Single Label (MAR-SL) in CG and XO; Mineral Surface versus Bone Surface (MS/BS), measured in the three ROIs both in CG and XO.

Parameter	2DHVP	CTRLs
BIC [%]	72,14 ± 2,36	62,19 ± 2,81
BIC fluo CG [%]	19,69 ± 2,85	8,54 ± 0,90
MAR-SL CG [µm/day]	8,49 ± 0,65	6,11 ± 0,54
MS/BS-CG ROI1 [%]	23,71 ± 2,34	15,75 ± 2,31
MS/BS-CG ROI2 [%]	15,30 ± 1,92	11,60 ± 1,42
MS/BS-CG ROI3 [%]	13,44 ± 1,95	10,68 ± 1,13
BIC fluo XO [%]	2,75 ± 0,42	3,48 ± 0,85
MAR-SL XO [µm/day]	4,60 ± 0,25	4,09 ± 0,19
MS/BS-XO ROI1 [%]	2,23 ± 0,44	4,36 ± 1,34
MS/BS-XO ROI2 [%]	2,19 ± 0,30	2,77 ± 0,77
MS/BS-XO ROI3 [%]	1,43 ± 0,39	1,98 ± 0,65

Figure 1: Schematic representation of implant functionalization. A: sand-blasted and acid-attacked cylinders , B: silanized surface, C: side-chain protected peptide anchored to the surface (red points represent the side-chain protecting groups; the blue trait represents glutaric anhydride spacer), D: peptide 2DHVP anchored to the surface. Letters refers to D-amino acids.

Figure 2: Rat skeleton (A) and enlargement of the left stifle in a lateral view (B) with the implant site (blue) in femur distal metaphysis. Sequence of intra-operative steps: incision of the skin (C), implant site preparation by the use of a trephine burr (D) and press fit implant insertion (E) and finally the implant located in the lateral portion of the femur' distal metaphysis (F). Schematic representation of the time course of bone markers administration.

Figure 3: Representative histological microphotograph of 2DHVP and CTRL implants stained with Goldner's trichrome at the end of the experimental time. Histological mirophotograph of the bone to implant interface: CTRL group (A,B,C,D) with a thin layer of bone in contact with the surface, stained with Goldner's trichrome (A,B), analysed under polarized light (C) and stained with Villanueva (D); 2DHVP group (E,F,G,H) with a newly formed bone at the implant interface stained with Goldner's trichrome (E,F), analysed under polarized light (G) and stained with Villanueva (H). Asterisks indicate newly formed bone; arrows indicate osteocytes lacunae. Scale bar 200 µm.

Figure 4: Representative fluorescent merge of bone markers Calcein Green (Green; 7-8 days) and Xylenol Orange (Red; 12-13 days) represent the osteogenic fronts of newly formed bone during each marker frame around the implant. CTRL (A) and 2DHVP (B) samples. Intensity Surface Plot of a 2DHVP (C) and a CTRL (D) samples derived from the measurement of the intensity of each pixel under fluorescence microscopy. Magnification of the originals images was 2X.

Figure 5: Histogram representing the BIC values of 2DHVP and CTRL groups at 15 days after the surgery (A). Histogram representing the osteogenic BIC (B) and MAR-SL (C) values of 2DHVP and CTRL group at both CG and XO time frame. Statistical significance: * $p<0,05$; **$p<0,001$.

Figure 6. (A) Schematic representation of the regions of interest (ROIs) of equivalent thickness (220 µm), used to measure the histomorphometrical parameters MS/BS. Region 1 (ROI1) is the circular area closest to cylinder surface; region 2 (ROI2) is the subsequent one; region 3 (R3) is the farthest from cylinder (*) implant. (B) Histogram of the MS/BS at the CG and XO time frame within the different ROIs. Statistical significance: * $p<0,05$; **$p<0,001$.

(C) Schematic representation of the regions used to evaluate the orientation of neodeposition. (D) Radar graph representing the distribution of the newly formed bone within the ROIs quadrant: Distal-Caudal, Distal-Cranial, Proximal-Caudal and Proximal-Cranial. ▲ indicate the ROI1, □ represent ROI2 and ● the ROI3.

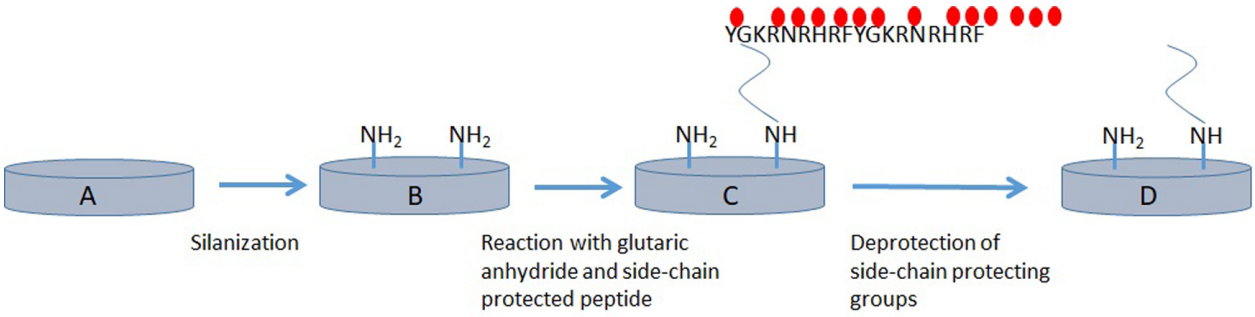

Figure 1

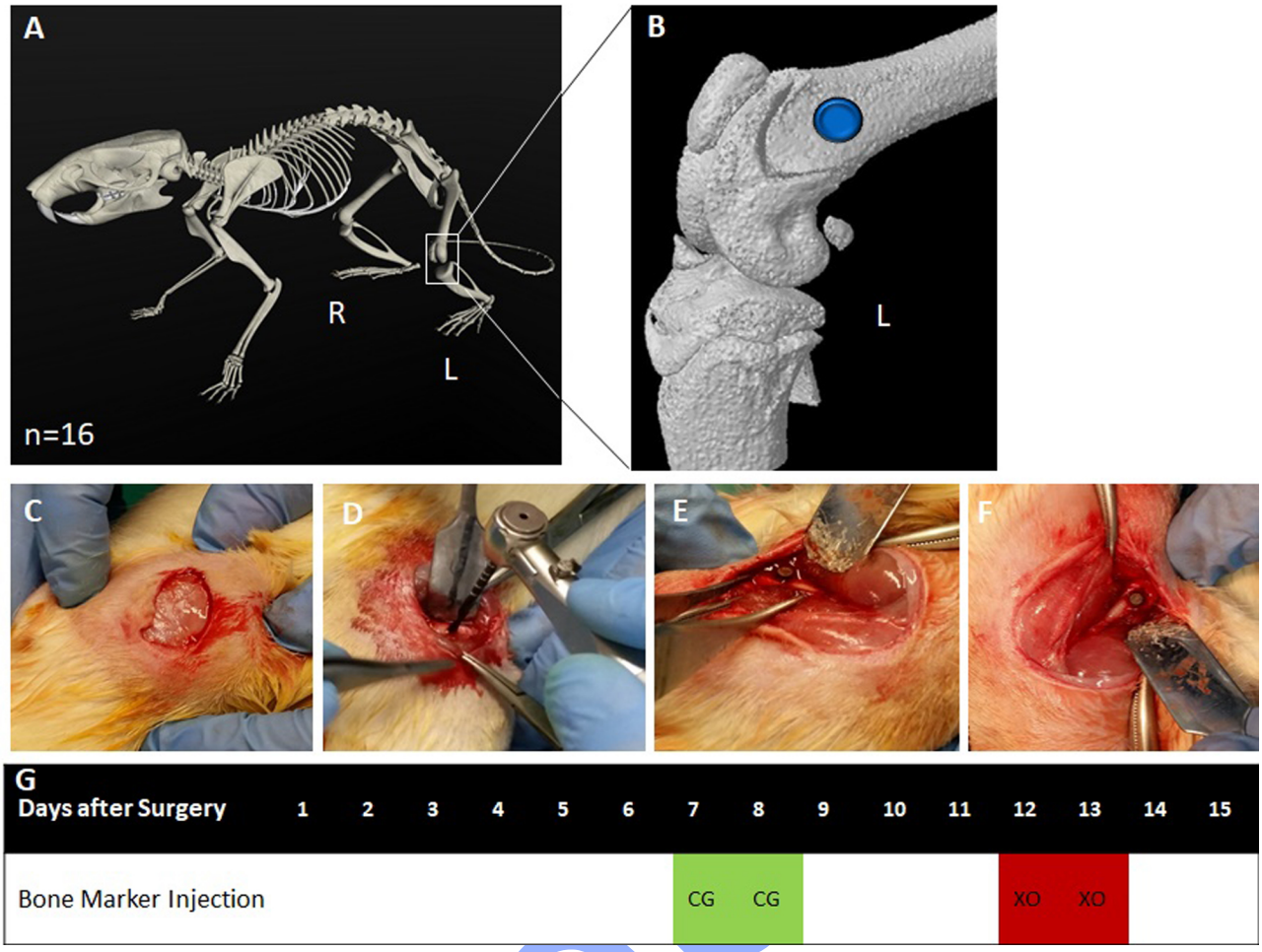

Figure 2

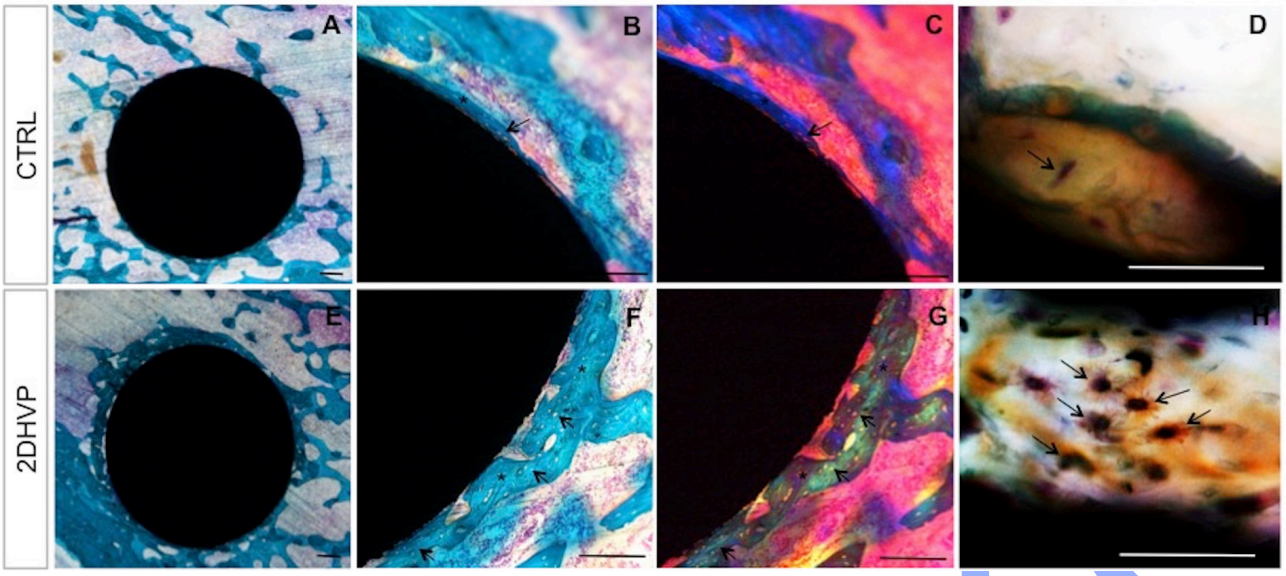

Figure 3

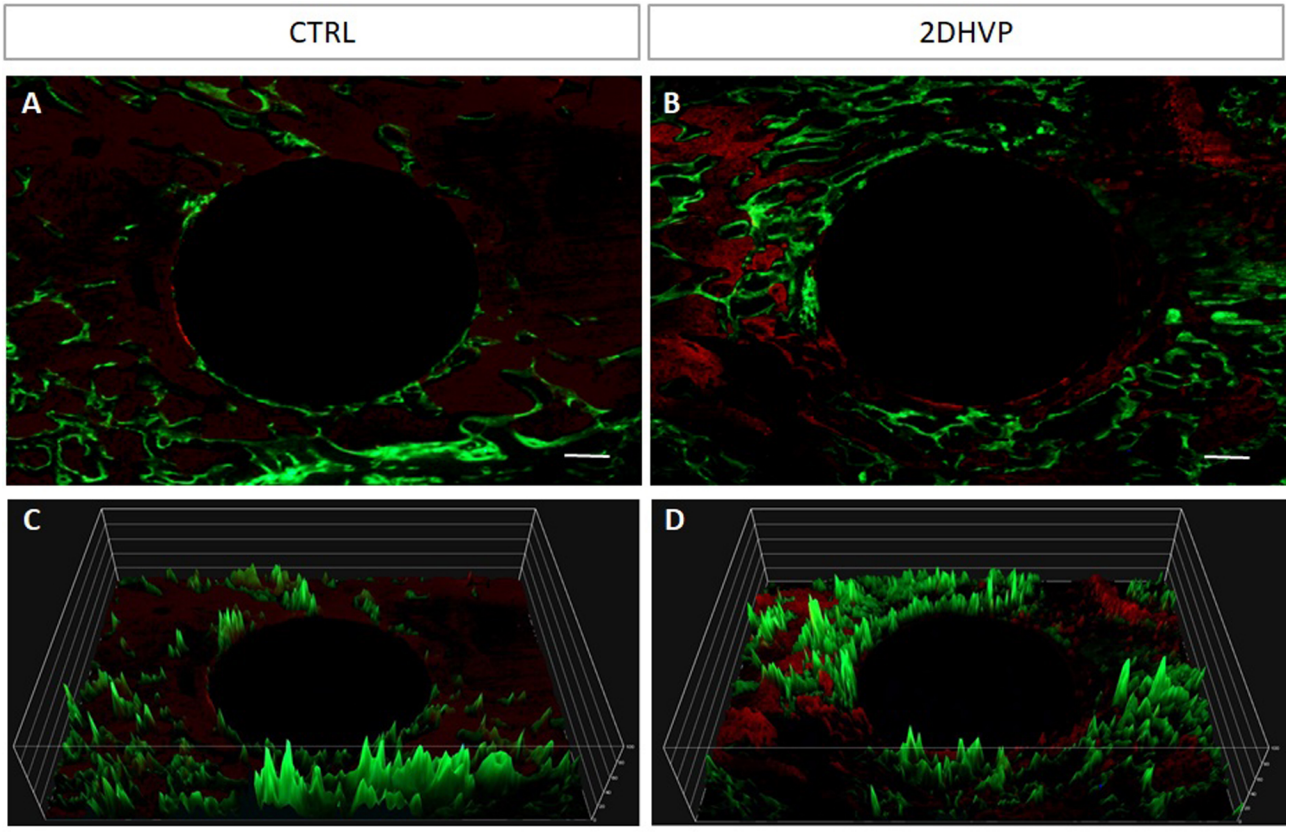

Figure 4

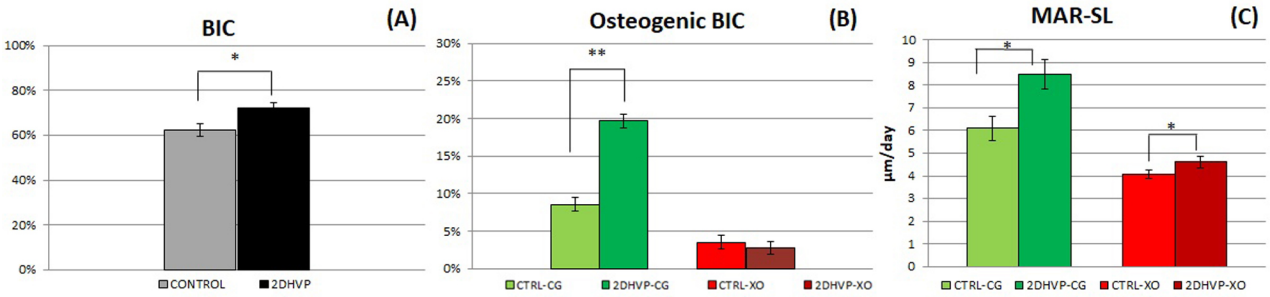

Figure 5

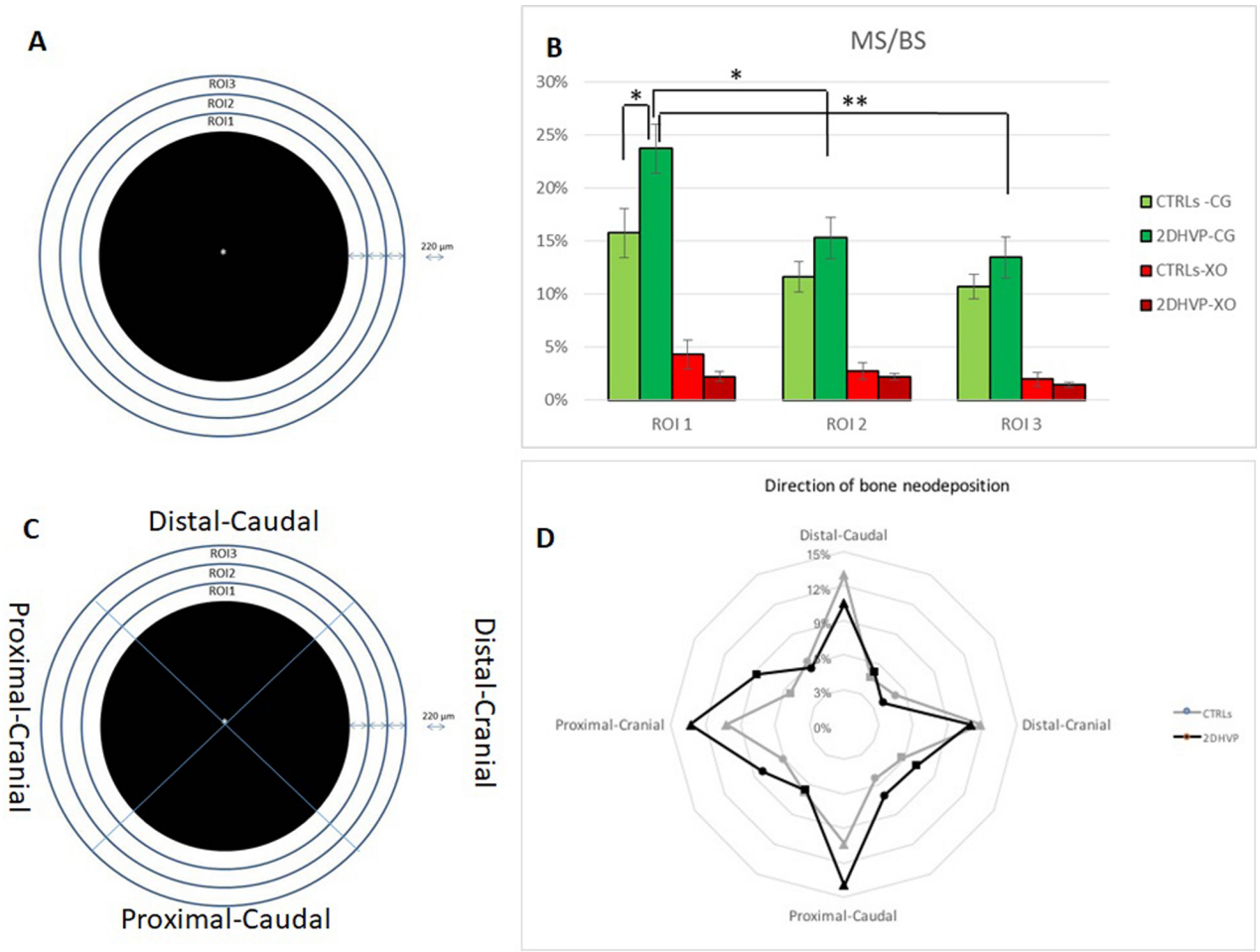

Figure 6